Title

Elongated galactan side chains mediate cellulose—pectin interactions in engineered Arabidopsis secondary cell walls

Journal

The Plant Journal, 115(2)

ISSN

0960-7412

Authors

Gao, Yu

Lipton, Andrew S

Munson, Coyla R

et al.

Publication Date

2023-07-01

DOI

10.1111/tpj.16242

the plant journal

SEB SOCIETY FOR EXPERIMENTAL BIOLOGY

The Plant Journal (2023) **115,** 529–545 doi: 10.1111/tpj.16242

Elongated galactan side chains mediate cellulose–pectin interactions in engineered Arabidopsis secondary cell walls

Yu Gao[1,2], Andrew S. Lipton[3], Coyla R. Munson[4], Yingxuan Ma[5,6], Kim L. Johnson[5,6], Dylan T. Murray[4], Henrik V. Scheller[1,2,7] and Jenny C. Mortimer[1,2,8,*]

[1]*Joint BioEnergy Institute, Emeryville, California 94608, USA,*
[2]*Environmental Genomics and Systems Biology Division, Lawrence Berkeley National Laboratory, 1 Cyclotron Road, Berkeley, California 94720, USA,*
[3]*Environmental Molecular Sciences Laboratory, Pacific Northwest National Laboratory, Richland, Washington 99354, USA,*
[4]*Department of Chemistry, University of California Davis, Davis, California 95616, USA,*
[5]*School of BioSciences, The University of Melbourne, Parkville, Victoria 3052, Australia,*
[6]*Department of Animal, Plant and Soil Sciences, La Trobe Institute for Agriculture and Food, La Trobe University, Bundoora, Victoria 3086, Australia,*
[7]*Department of Plant and Microbial Biology, University of California Berkeley, Berkeley, California 94720, USA, and*
[8]*School of Agriculture, Food and Wine, Waite Research Institute, Waite Research Precinct, University of Adelaide, Glen Osmond, South Australia 5064, Australia*

Received 4 August 2021; revised 23 March 2023; accepted 25 March 2023; published online 8 April 2023.
*For correspondence (e-mail jenny.mortimer@adelaide.edu.au).

SUMMARY

The plant secondary cell wall is a thickened matrix of polysaccharides and lignin deposited at the cessation of growth in some cells. It forms the majority of carbon in lignocellulosic biomass, and it is an abundant and renewable source for forage, fiber, materials, fuels, and bioproducts. The complex structure and arrangement of the cell wall polymers mean that the carbon is difficult to access in an economical and sustainable way. One solution is to alter the cell wall polymer structure so that it is more suited to downstream processing. However, it remains difficult to predict what the effects of this engineering will be on the assembly, architecture, and properties of the cell wall. Here, we make use of Arabidopsis plants expressing a suite of genes to increase pectic galactan chain length in the secondary cell wall. Using multi-dimensional solid-state nuclear magnetic resonance, we show that increasing galactan chain length enhances pectin–cellulose spatial contacts and increases cellulose crystallinity. We also found that the increased galactan content leads to fewer spatial contacts of cellulose with xyloglucan and the backbone of pectin. Hence, we propose that the elongated galactan side chains compete with xyloglucan and the pectic backbone for cellulose interactions. Due to the galactan topology, this may result in comparatively weak interactions and disrupt the cell wall architecture. Therefore, introduction of this strategy into trees or other bioenergy crops would benefit from cell-specific expression strategies to avoid negative effects on plant growth.

Keywords: *Arabidopsis thaliana*, secondary cell wall, pectin, galactan, solid state nuclear magnetic resonance, biofuels, recalcitrance.

INTRODUCTION

The plant cell wall is a complex matrix of polysaccharides and lignin. The thin extensible primary wall surrounds every cell, giving the cell shape, while the middle lamella mediates cell–cell adhesion. The thickened secondary cell wall, which is laid down at the cessation of cell expansion in some cell types, provides support and defense from pathogens and herbivores (Caffall & Mohnen, 2009; Gondolf et al., 2014; Scheller et al., 2006). The secondary cell wall is also the dominant component in most lignocellulosic biomass, so it is the primary store of photosynthetically fixed carbon in most terrestrial ecosystems. Historically, the secondary cell wall has also provided materials, dietary fiber, and animal forage for human needs. The urgent requirement to reduce the carbon emissions from use of fossil resources while fulfilling the growing global demand for fuels, chemicals, and materials has placed the cell wall as a key carbon resource to support

sustainable biotechnology (Mahajan et al., 2020; Marriott et al., 2016; Zhu et al., 2020).

In dicots, such as *Arabidopsis thaliana* (Arabidopsis) and *Populus* spp. (poplar), the secondary cell walls are mainly composed of cellulose, xylan, and lignin, with smaller amounts of pectin and xyloglucan. Cellulose consists of β-1,4-linked glucan chains that are assembled in parallel via inter- and intramolecular hydrogen bonding to form crystalline microfibrils, which serve as the major load-bearing component of the wall (Dupree et al., 2015; Sorek et al., 2014). Cellulose can be categorized into two major domains (crystalline and amorphous), due to the imperfect order of cellulose crystallites (Atalla & Vanderhart, 1984, 1999; Gao et al., 2020). In dicots, the major hemicellulose in secondary walls is xylan, which consists of a linear backbone of β-1,4-linked xylosyl units substituted with α-1,2-glucuronosyl or α-1,2-(4-*O*-methyl)-glucuronosyl units (Rennie & Scheller, 2014). The xylosyl units from the xylan backbone can also be acetylated at the *O*-2 and *O*-3 positions (Rennie & Scheller, 2014). The pattern of substitutions on the xylan backbone plays a critical role in determining xylan conformation (two-fold screw [180° bond angle] or three-fold screw [120° bond angle] conformations) and affects interactions with other wall components in the Arabidopsis secondary cell walls (Bromley et al., 2013; Busse-Wicher et al., 2014; Dupree et al., 2015; Simmons et al., 2016). Although xyloglucan is the major hemicellulose in dicot primary cell walls, only a minor amount is present in the secondary cell walls (Scheller & Ulvskov, 2010). Xyloglucan has a β-1,4-linked glucan backbone, which is substituted with repetitive units, including D-xylosyl, D-galactosyl, and D-fucosyl sugars (Scheller & Ulvskov, 2010). Like xyloglucan, pectin is a major component of the primary cell wall and a minor component of the secondary cell wall (Willats et al., 2001). Pectin has three main domains: homogalacturonan (HG, 65%), rhamnogalacturonan-I (RG-I, 20–30%), and rhamnogalacturonan-II (RG-II, 10%) (Caffall & Mohnen, 2009; Marriott et al., 2016; Scheller et al., 2006; Willats et al., 2001). HG consists of α-1,4-linked galacturonosyl units which are often methylesterified at *O*-6 and acetylated at *O*-2 and *O*-3 (Scheller et al., 2006). RG-I has a backbone consisting of the repeating disaccharide α-1,4-galacturonic acid–α-1,2-rhamnose, where the rhamnosyl units are often substituted with chains of galactan (β-1,4-linked), arabinan (α-1,5-linked), and arabinogalactan (β-1,4-linked galactan with arabinan branches) (Caffall & Mohnen, 2009; Scheller et al., 2006). The RG-II backbone is also formed of α-1,4-linked galacturonosyl units, but clusters of complex side chains (composed of 12 types of glycosyl units and at least 22 glycosidic bonds) are substituted at the *O*-2 or *O*-3 positions (Caffall & Mohnen, 2009; Scheller et al., 2006).

One of the major barriers to using lignocellulosic biomass as a resource for the bioeconomy is the high recalcitrance of the cell wall (Gao et al., 2016; Loqué et al., 2015; Marriott et al., 2016; Sorek et al., 2014). Microbial conversion to desirable products requires simple carbon sources, and the release of carbon from biomass is challenging to do in a sustainable and economic manner. One approach is to design and develop dedicated bioenergy crops, employing genetic engineering to alter the composition of plant cell walls with desired traits beyond that which is possible via conventional breeding (Aznar et al., 2018; Eudes et al., 2015; Hao et al., 2021; Loqué et al., 2015; Smith et al., 2017). One such strategy is to develop plant cell walls with higher hexose/pentose ratios, since hexose is more easily utilized during microbial conversion (Loqué et al., 2015). Previously, we have improved the hexose/pentose ratio by enhancing the pectic galactan content in Arabidopsis secondary cell walls (Aznar et al., 2018; Yan et al., 2018). This was achieved by co-expressing *UDP-GLUCOSE EPIMERASE* (*UGE*), which encodes a cytosolic enzyme, *UDP-RHAMNOSE/UDP-D-GALACTOSE TRANSPORTER 1* (*URGT1*), which encodes a Golgi protein, and *GALACTAN SYNTHASE 1* (*GALS1*), which encodes a Golgi-localized β-1,4-galactosyltransferase, under the control of secondary cell wall-specific promoters. The pectic galactan content was increased by 50% in the transgenic Arabidopsis stem tissue, and the plants did not show any apparent growth defects (Aznar et al., 2018). Immunofluorescence microscopy showed the presence of galactan-reactive epitopes in thickened stem cell walls (Gondolf et al., 2014). How this increase in pectic galactan would direct architectural alterations in the plant cell wall and aid in reducing recalcitrance during lignocellulose processing remains to be seen.

Exploring the native structure of plant cell walls is challenging, since most methods (such as mass spectrometry) require some form of pre-treatment, which disrupts the wall arrangement. An exception to this is solid-state nuclear magnetic resonance (ssNMR), which does not require disruptive sample preparation. ssNMR using plant material with a near-saturating content of ^{13}C allows us to directly monitor the structural details of wall components at the molecular level and study the 3D network formed by the interactions between these components (Dick-Pérez et al., 2011; Gao et al., 2020; Kang et al., 2019; Simmons et al., 2016; Terrett et al., 2019). However, most studies on the role of pectin using ssNMR focus on the primary cell wall (Dick-Pérez et al., 2012; Wang & Hong, 2016, 2017; Wang, Park, et al., 2015). For example, in the Arabidopsis primary cell wall, extensive pectin–cellulose interactions were identified, suggesting that pectin plays a role in maintaining structural integrity (Dick-Pérez et al., 2011), and subsequent work suggested that it is the pectic backbone rather than the side chains which interact with cellulose to regulate wall extensibility (Phyo et al., 2017). However, in sugar beet (*Beta vulgaris*) and potato (*Solanum tuberosum*) cell walls, evidence for binding of pectic side chains to cellulose has been reported (Zykwinska et al., 2005). The

interactions between pectic side chains and cellulose are generally weaker than those between xyloglucan and cellulose, due to conformational inefficiency. However, the less branched pectic side chains (e.g., arabinans and galactans) mediate a relatively strong binding with cellulose, as compared to highly branched side chains, due to less steric hindrance (Zykwinska et al., 2005, 2008). Additionally, Moneo-Sánchez et al. (2020) recently reported that reduced pectic galactan content results in increased xyloglucan–cellulose interactions during secondary cell wall deposition. This suggests that pectic galactan could play a key role in regulating xyloglucan–cellulose interactions in the secondary cell wall, despite its low abundance.

Here, we used a series of multi-dimensional ssNMR experiments to explore the effects of modulating galactan chain length on the architecture of the secondary cell wall. This in turn allowed us to better understand the role of pectic galactan in wild-type secondary cell walls. We show that pectin has a limited role in maintaining the structural integrity of the secondary cell wall, unlike in the primary cell walls. The elongated galactan chains in the engineered Arabidopsis closely associate with cellulose and limit interactions of cellulose with xyloglucan and pectin backbones, thereby loosening the cell wall matrix (Dick-Pérez et al., 2012; Kirui et al., 2021; Wang et al., 2012; Wang, Park, et al., 2015).

RESULTS

Secondary cell wall-enriched stem tissue is used for ssNMR

To investigate the architecture of secondary cell walls, stem tissue from both the wild-type and engineered high galactan Arabidopsis was used for ssNMR analysis. The stem tissue material is a mixture of all cell wall types, and complete separation of primary wall and middle lamella from secondary wall in the plant tissue is challenging. This is particularly true if, as is the goal of this investigation, the physical relationship between different cell wall components is to be maintained. Hence, to confirm that the stem tissue used for this study is highly enriched in secondary cell walls, we performed monosaccharide composition analysis of our stem samples (Figure S1). Analysis of the non-cellulosic fraction revealed that the cell wall samples are dominated by xylose, with relatively low quantities of glucose, galacturonic acid, and other characteristic pectic monosaccharides. Additionally, we also determined that the Klason lignin content of the stem tissue we used for this study is comparable to published data from secondary cell wall-rich tissue of mature Arabidopsis (Table S1). Thus, the Arabidopsis stem samples we used were highly enriched with secondary cell walls by percent biomass.

Plants engineered for increased secondary cell wall pectic galactan show an increased signal in the neutral polysaccharide region of one-dimensional direct polarization NMR

To gain an overview of the secondary cell wall-enriched components in both the wild-type (control) and the high galactan Arabidopsis, we first performed quantitative one-dimensional (1D) direct polarization (DP) experiments with a long recycle delay (30 sec) on the ^{13}C-stem samples (Figure 1). All plants were grown in an atmosphere with a very high $^{13}CO_2/^{12}CO_2$ ratio to enable detection of C–C correlations that would be undetectable with the natural occurrence of ^{13}C. Only the bottom part of mature inflorescence stems was sampled to ensure the tissue was highly enriched in secondary cell wall. To enable comparison between the two samples, the spectra were adjusted to the same overall integral intensity. Four major regions (carbonyls, lignin, polysaccharides, and proteins) are annotated according to previous reports (Dupree et al., 2015; Wang et al., 2012). Peaks are assigned based on previous reports (Table S2) and are labeled according to the following nomenclature as an example: ^{C}C4 is carbon 4 of the glucosyl unit from crystalline cellulose, where the superscript $^{[C]}$ represents the crystalline domain. As expected due to the enhanced galactan content, the high galactan line has higher intensity peaks in the polysaccharide region. However, all six carbon signals of galactan (Gal1–6) overlap with the signals from cellulose (C1 at approximately 105 ppm, C2, C3, and C5 at region 70–80 ppm, and C6 at region 61–65 ppm), so from the 1D spectra alone, it is unknown whether the increase in signal intensity is from galactan alone or other cell wall components have also changed.

Only RG-I galactan signals are significantly enhanced in two-dimensional ssNMR experiments

Due to the overlap of the polysaccharide signals in the 1D spectra, we conducted two-dimensional (2D) double-quantum (DQ) and single-quantum (SQ) ^{13}C–^{13}C correlation experiments using the refocused INADEQUATE sequence. Cross peaks in these spectra arise from directly bonded carbon nuclei. The DQ chemical shift is the sum of the chemical shifts for the nuclei involved in the bond and the SQ chemical shifts report on the chemical identities of the individual nuclei. The multi-dimensional experiments allow us to better resolve the resonances and investigate individual cell wall components.

The INADEQUATE experiments with DP and short recycle delay (2 sec), which preferentially detects relatively mobile components from the cell wall, were performed on both the wild-type and the high galactan samples. The chemical shift regions of 110–60 ppm on the SQ dimension and 200–130 ppm on the DQ dimension are where most of

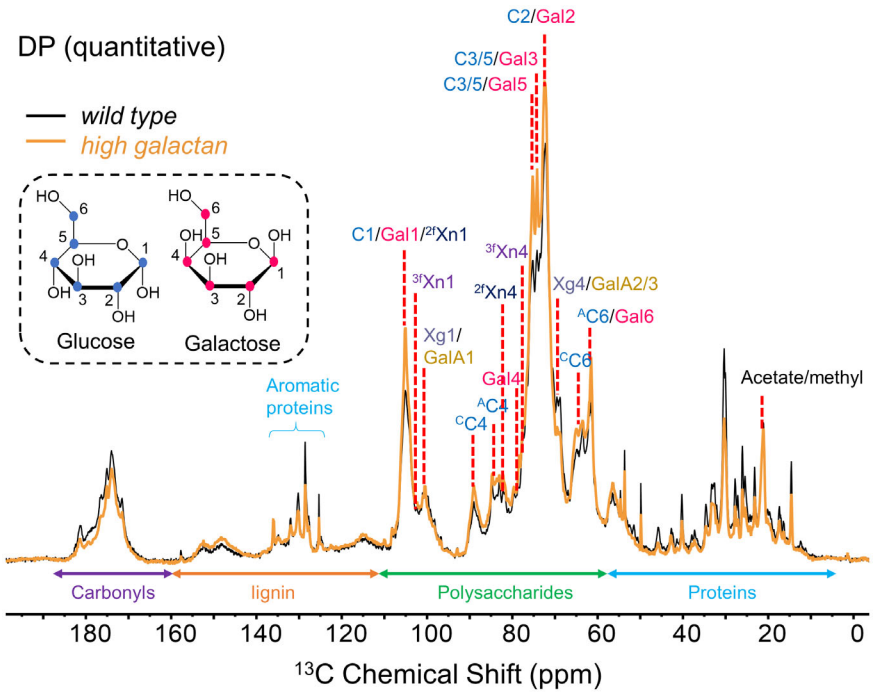

Figure 1. Overlaid quantitative one-dimensional magic angle spinning (MAS) solid-state ^{13}C nuclear magnetic resonance direct polarization spectra of the wild-type and high galactan samples collected with a recycle delay of 30 sec.
Spectra were scaled to intensities with similar total integrals for general comparison of wall components between the two samples. Four major regions (carbonyls, lignin, polysaccharides, and proteins) were assigned. The peaks of glucosyl units from cellulose are labeled as C, where the superscripts [C] and [A] represent the crystalline and amorphous domains of cellulose, respectively; the peaks of xylosyl units from xylan are labeled as Xn, where the superscripts [2f] and [3f] represent the two-fold screw and three-fold screw conformations, respectively; the peaks of galactosyl units from galactan are labeled as Gal; peaks of galacturonosyl units from the pectic backbone are labeled as GalA; and the peaks of xylosyl units from xyloglucan are labeled as Xg.

the resonances of relatively mobile polysaccharides from pectin and hemicelluloses are located. Figure 2(a) shows the overlay of this region from the spectra of the wild-type and high galactan samples. As the dominant hemicellulose in the secondary cell walls, a significant amount of xylan in three-fold screw conformation (^{3f}Xn1–5, where superscript [3f] represents a xylosyl unit in the three-fold screw conformation) was detected in both the wild-type and the high galactan samples due to its relatively mobile nature. Two carbons of the glucuronosyl units that substitute the xylan backbone, denoted as GlcA1 and GlcA2, were also identified. Carbons 1 and 2 from the mannosyl units of mannan (Man1–2) and acetylated mannan (^{Ac}Man1–2, where superscript [Ac] represents acetylated) were also detected in low abundance in both samples. Signals of xylosyl units from relatively mobile xyloglucan (e.g., Xg4, Xg5) were identified, showing significantly reduced mobile xyloglucan content in the high galactan sample relative to the wild-type sample.

Two sets of cross peaks representing carbon 1 and carbon 2 from galacturonosyl units, likely derived from the pectic backbone, were distinguished. We have labeled them as ^{a,b}GalA1–2, where superscripts [a] and [b] represent the cross peak sets (Figure 2c). Carbon 1 and carbon 2 of the rhamnosyl units from the RG-I backbone, denoted as Rha1 and Rha2, were identified. Three sets of signals from arabinosyl units ($^{a–c}$A1–5, where superscripts [a–c] represent the three types) were identified in both samples. The three types are primarily distinguished by the chemical shifts of carbon 5. The ^{a}A units, which have an ^{a}A5 chemical shift of 62.5 ppm, are assigned as the terminal units from pectic arabinan side chains (Figure 2c). Both ^{b}A5 (67.9 ppm) and ^{c}A5 (64.2 ppm) show significant shift to lower shielding compared to ^{a}A5, so ^{b}A and ^{c}A are assigned as the 5-linked arabinosyl units from pectic arabinan side chains (Wang et al., 2014).

Three sets of galactosyl units ($^{a–c}$Gal1–6) were also identified from both samples. ^{c}Gal is identified as substituent units from xyloglucan (Dick-Pérez et al., 2011). ^{a}Gal and ^{b}Gal are derived from pectic galactan (Larsen et al., 2011; Mikshina et al., 2012; Phyo et al., 2017; Wang et al., 2014; Zykwinska et al., 2006), but they show very distinct chemical shifts at carbon 4. ^{a}Gal4 has a significant downfield chemical shift at 78.5 ppm as compared to ^{b}Gal4 at 69.5 ppm, so ^{a}Gal can be assigned to 4-linked units and ^{b}Gal to terminal units (Wang et al., 2014). Supporting this assignment, the high galactan sample shows a much stronger signal from ^{a}Gal than the wild-type sample, while

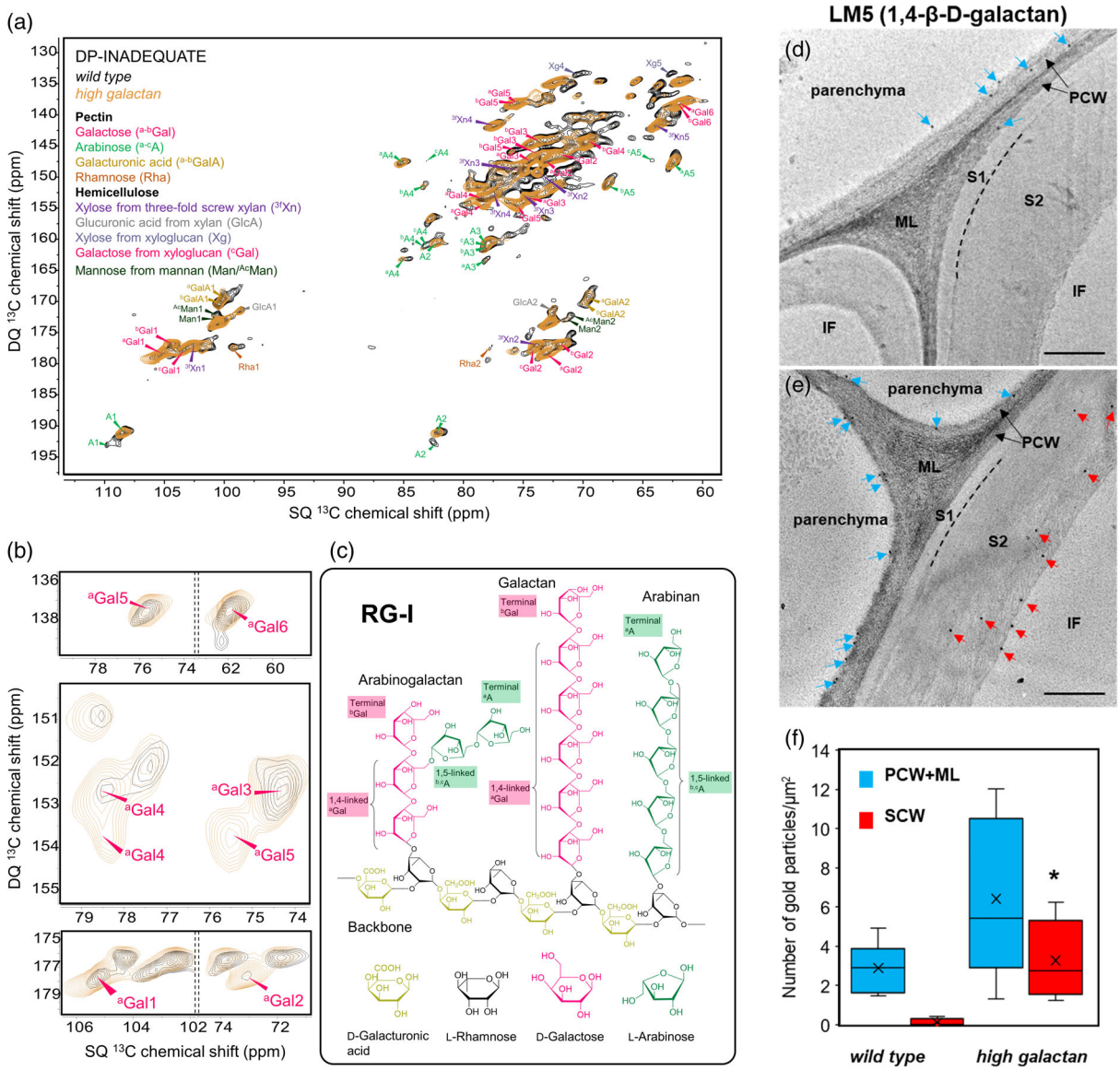

Figure 2. (a) Overlaid DP-INADEQUATE spectra of the wild-type (black) and the high galactan (orange) Arabidopsis stem material at the major polysaccharide region. Polysaccharides from pectin and the relatively mobile fraction of hemicellulose were assigned and reported in Table S2 according to literature (Dick-Pérez et al., 2011, 2012; Phyo et al., 2017; Simmons et al., 2016; Terrett et al., 2019; Wang et al., 2014), including two sets of signals from galacturonosyl units (^{a,b}GalA), three sets of signals from galactosyl units ($^{a-c}$Gal), three sets of signals from arabinosyl units ($^{a-c}$A), signals from xylosyl units in xyloglucan (Xg) and in three-fold screw xylan (^{3f}Xn), and two sets of signals from mannosyl units from mannan (Man) and acetylated mannan (^{Ac}Man). A higher resolution version of panel (a) is included as Figure S12.

(b) Zoom-in windows of overlaid DP-INADEQUATE spectra in three regions showing significantly enhanced signals from ^{a}Gal1–6 in the high galactan sample and assigned distinct sets of signals from galactosyl units of galactan ($^{a-b}$Gal) are shown in Figure S2.

(c) Simplified schematic structure of RG-I with galactan, arabinan, and arabinogalactan side chains.

(d, e) Location of pectic galactan in interfascicular fiber (IF) cells at the base region of stems. TEM immuno-labeling detection of pectic 1,4-β-D-galactan (LM5 antibody) in transverse sections at 1 cm from the stem base of stage 6.9 (Boyes et al., 2001) wild-type (d) and high galactan (e) plants. Blue arrows indicate gold particles in parenchyma cell primary walls (PCWs), red arrows indicate gold particles in IF secondary walls (SCWs). Scale bar = 500 nm. ML, middle lamella; S1 and S2, secondary wall layers S1 and S2.

(f) Quantification of gold particles/mm^2 cell wall area for epitopes detected by LM5 antibody in parenchyma PCWs and IF SCWs of wild-type and high galactan plants. *P < 0.05 compared to wild type (Student's t-test).

the signals of ^{b}Gal remain similar between the two samples (Figure 2b; Figure S2). To verify that the plant tissue collected for these experiments recapitulated the previously reported biochemical data (Aznar et al., 2018), we determined the non-cellulosic monosaccharide composition. In the high galactan line, consistent with previous

reports, there was a significant increase in galactose (Figure S1).

The enhancement of galactan in these lines, as previously reported (50%), was achieved by the co-expression of *GALS1* (encoding galactan synthase), *UGE2* (encoding UDP-Glc epimerase), and *URGT1* (encoding a UDP-Rha/Gal Golgi transporter) under the control of secondary cell wall-specific promoters. Fluorescence immunohistochemistry of transverse stem sections showed increased galactan labeling in cell types which have a secondary cell wall (Aznar et al., 2018). To confirm that galactan was specifically increased in the secondary cell wall, as opposed to the primary cell wall or middle lamella, we used immunogold labeling with antibody LM5 to visualize 1,4-β-galactan epitopes in the transverse sections of the stem tissues (1 cm from the stem base) by transmission electron microscopy (TEM).

In the wild-type and high galactan lines, no significant differences in immuno-gold labeling of 1,4-β-galactan epitopes were detected in primary cell walls and the middle lamella (Figure 2d,f). In contrast, in the high galactan line, gold particles were frequently detected in the secondary cell wall of interfascicular fibers, with barely detectable labeling in wild type (Figure 2e,f). Increased gold labeling of 1,4-β-galactan epitopes only in secondary walls of high galactan lines was observed in interfascicular fiber, xylem vessel, and parenchyma cells from two biological replicates of both wild-type and high galactan samples (Figures S3–S6). Little to no gold labeling was observed in the control transverse sections incubated with no primary antibody (Figure S7) and no differences in gold labeling with the CCRC-M35 antibody (Pattathil et al., 2010), which detects pectin RG-I epitopes, were observed (Figures S8–S11).

In addition, INADEQUATE experiments with cross-polarization (CP) were also performed to detect the more rigid cell wall components (e.g., cellulose, two-fold screw xylan, and xyloglucan). The resulting spectra were overlaid (Figure S13), with all assignments also available in Table S2. In total, eight allomorphs of cellulose were assigned into two main domains (i.e., crystalline domain [^{C}C] and amorphous domain [^{A}C]) which show major chemical shift differences between ^{C}C4,6 and ^{A}C4,6. Three individual glucosyl units ($^{1-3A}$C) were assigned as belonging to the amorphous domain, and five glucosyl units ($^{1-5C}$C) were assigned as belonging to the crystalline domain. There was a decrease in the signals from the xylosyl units in xyloglucan, which indicates that less rigid xyloglucan was detected in the high galactan sample compared to the control (Figure S13).

Increasing pectic galactan in the secondary cell wall enhances spatial contacts between RG-I galactan and cellulose

To further explore how the elongated RG-I galactan chains changes cell wall architecture, we performed ^{13}C–^{13}C correlated proton driven spin diffusion (PDSD) experiments, which detect the carbons correlated through space. The PDSD experiments were conducted with both DP and CP to reveal proximities between mobile and rigid components respectively at three different mixing times (30, 100, and 1000 msec). When a shorter mixing time is used, only carbons separated by a shorter spatial distance will be detected.

The DP-PDSD experiments with a short mixing time (30 msec) and a short recycle delay (2 sec), which detect mainly intramolecular spatial contacts between relatively mobile wall components, were overlaid for comparison (Figure S14). As expected, the cross peak representing intramolecular spatial contacts between ^{a}Gal6 from the horizontal dimension (direct detect, F_2 dimension) and ^{a}Gal1 from the vertical dimension (indirect detect, F_1 dimension) denoted as ^{a}Gal6–^{a}Gal1 (61.9 ppm, 105.1 ppm) shows greater peak intensity in the high galactan sample than in the control. This enhancement of galactan intramolecular contacts is consistent with our DP-INADEQUATE results (Figure 2). Since this form of galactan is one of the side chains on RG-I pectin, enhanced signals representing spatial contacts between galactosyl units from galactan and galacturonosyl units from the RG-I backbone were also detected in the high galactan sample, such as ^{b}GalA4–^{a}Gal1 (79.2 ppm, 105.1 ppm), ^{b}GalA3–^{a}Gal1 (70.2 ppm, 105.1 ppm), and ^{b}GalA2–^{a}Gal1 (69.8 ppm, 105.1 ppm). Also, the high galactan sample shows increased cross peak intensity at ^{a}Gal5–^{4C}C4 (75.5 ppm, 89.1 ppm), ^{a}Gal3–^{4C}C4 (74.3 ppm, 89.1 ppm), ^{a}Gal5–^{2A}C4 (75.5 ppm, 84.3 ppm), ^{a}Gal3–^{2A}C4 (74.3 ppm, 84.3 ppm), and ^{a}Gal6–^{1,2A}C6 (61.9 ppm, 62.1 ppm) as compared to the wild-type control. This suggests a closer proximity of spatial contacts between pectic galactan and cellulose in the secondary cell walls of the high galactan sample. Additionally, the 1D slices extracted from the DP-PDSD with short mixing time at the arabinan carbons, ^{b,c}A4 (83.3 ppm) and ^{a}A4 (85.1 ppm), show increased peak intensities from ^{a}Gal only in the high galactan sample, suggesting increased dipolar contacts between galactan and arabinan.

To better compare the intermolecular interactions between the cell wall components, CP-PDSD experiments with T_1-relaxation compensated z-filter, which makes the total z-period a constant of 1.005 sec (Wang, Williams, et al., 2015), were also performed at both short (200 msec) and long (1000 msec) mixing times. The obtained spectra with short (200 msec) mixing time, which detects most intramolecular spatial contacts, and with long (1000 msec) mixing time, which detects both intra- and intermolecular spatial contacts, were overlaid (Figure 3a,b). Taking the difference of these spectra removes the contributions from the intramolecular contacts, leaving only the intermolecular spatial contacts. The overlaid difference PDSD spectrum of the two samples is provided as Figure S15 in the

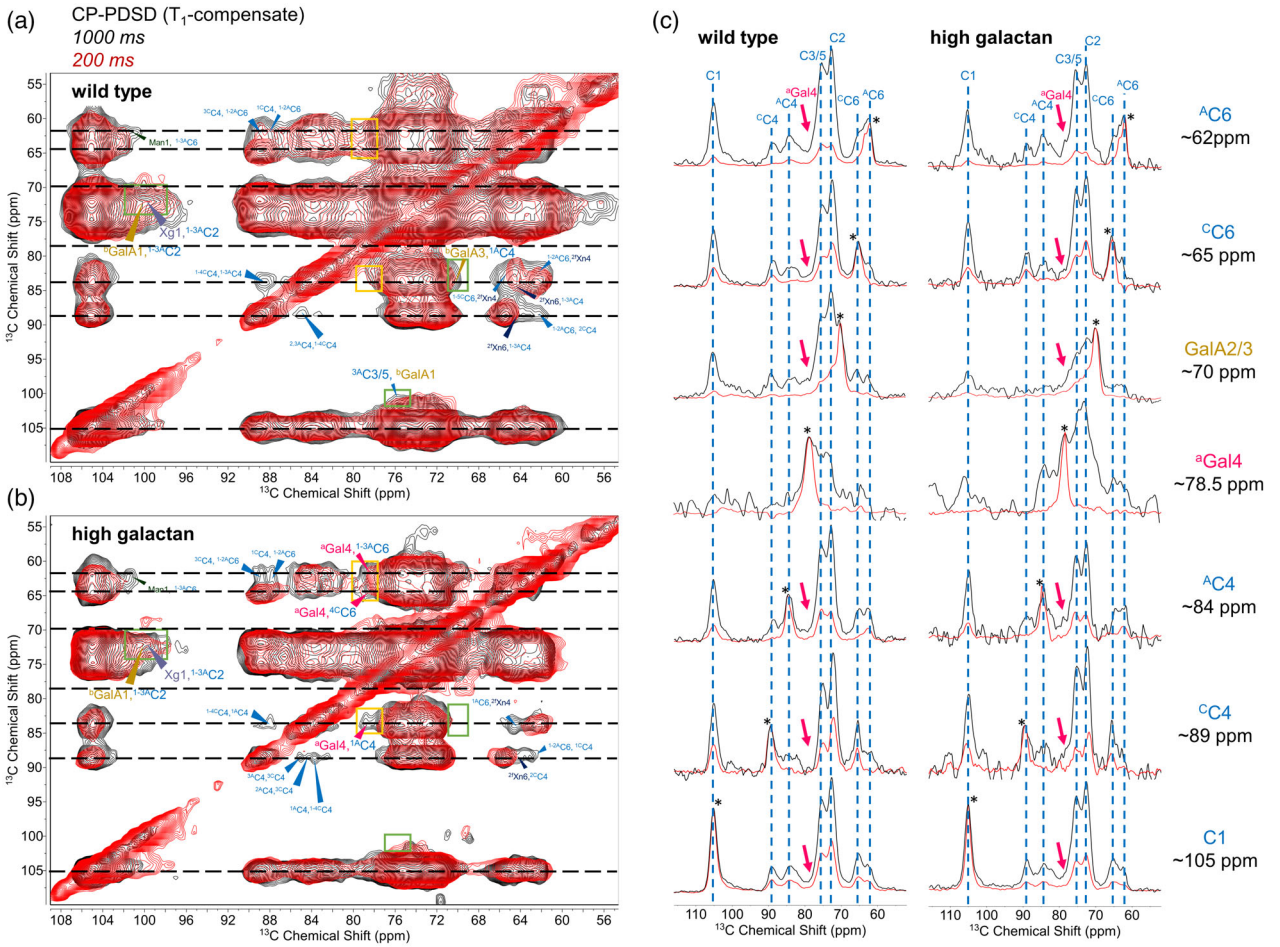

Figure 3. Overlaid T_1-compensated proton driven spin diffusion (PDSD) spectra with mixing times of 200 and 1000 msec.
(a) Obtained using a scaling factor of 0.82 for the 200 msec spectrum for the wild-type sample.
(b) Obtained using a scaling factor of 0.74 for the 200 msec spectrum for the high galactan sample. The yellow boxes compare spatial contacts between galactan and cellulose and the green boxes compare spatial contacts between the pectic backbone or xyloglucan and cellulose in the wild-type and high galactan samples.
(c) One-dimensional slices extracted from the F_2 dimension at seven chemical shifts from the F_1 dimensions of the T_1-compensated PDSD spectra of the wild-type and high galactan samples with mixing times of 200 and 1000 msec.

supplementary information. The characteristic chemical shift of galactan, ^{a}Gal4 (78.5 ppm), is exceptionally useful to identify contacts between galactan and other wall components. The high galactan sample shows significantly increased cross peak intensity at ^{a}Gal4–^{1A}C4 (78.5 ppm, 83.8 ppm), ^{a}Gal4–$^{1-3A}$C6 (78.5 ppm, 62 ppm), and ^{a}Gal4–^{4C}C6 (78.5 ppm, 64.9 ppm) compared to the wild-type control as denoted in the yellow boxes in Figure 3(a, b). This indicates that the extended galactan chains are found in close proximity to cellulose.

To better illustrate spatial contacts between galactan and the other wall components, 1D slices on the horizontal dimension were extracted at seven chemical shifts, which represent ^{A}C6 (62 ppm), ^{C}C6 (65 ppm), GalA2/3 (70 ppm), ^{a}Gal4 (78.5 ppm), ^{A}C4 (84 ppm), ^{C}C4 (89 ppm), and C1 (105 ppm) from the vertical dimension of spectra with two different mixing times (200 and 1000 msec) for both the wild-type (Figure 3c, left column) and the high galactan (Figure 3c, right column) samples. The 1D extracts with mixing times of 200 and 1000 msec were overlaid at each selected chemical shift, and the intensity of the spectra was normalized to the same selected chemical shift from which they were extracted, as indicated with an asterisk. The 1D slices with a mixing time of 1000 msec extracted at characteristic cellulose carbons, C1 (105 ppm), ^{A}C4/6 (approximately 84/62 ppm), ^{C}C4/6 (approximately 89/65 ppm), and the characteristic pectic backbone carbon, GalA2/3 (approximately 70 ppm), all demonstrated an increase in the peak intensity at ^{a}Gal4 (78.5 ppm) for the high galactan sample compare to the wild-type control, which is indicated with the pink arrows in Figure 3(c). Further, the 1D slices extracted at ^{a}Gal4 (78.5 ppm) also show

significantly enhanced intensities of all cellulose peaks C1 (105 ppm), C2/3/5 (approximately 72–76 ppm), ^{A}C4/6 (approximately 84/62 ppm), and ^{C}C4/6 (approximately 89/65 ppm). This supports our interpretation that extending the galactan chain lengths in the secondary cell wall increases spatial contacts between galactan and both amorphous and crystalline cellulose.

Increased secondary cell wall galactan reduced the rigid spatial contacts between pectin and cellulose

In contrast to the enhanced galactan and cellulose spatial contacts in the high galactan sample, the T_1-compensated CP-PDSD spectra (Figure 3a,b; Figure S15) also show fewer intermolecular cross peaks between the galacturonosyl units from the pectic backbone and the glucosyl units from cellulose as compared to the control. This includes ^{b}GalA1–^{3A}C3/5 (100.2 ppm, 75.8 ppm), ^{b}GalA1–$^{1–3A}$C2 (100.2 ppm, 72.7 ppm), and ^{b}GalA3–^{1A}C4 (70.2 ppm, 83.8 ppm) as indicated in the green boxes in Figure 3(a,b). To better observe the close spatial contact between the galacturonosyl units and other carbons, the 1D slices with a mixing time of 1000 msec were extracted at the characteristic pectic backbone carbon, GalA2/3 (approximately 70 ppm), as demonstrated in Figure 3(c). The spectra show greatly reduced intensities at all cellulose peaks, including C1 (105 ppm), C2/3/5 (approximately 72–76 ppm), ^{A}C4/6 (approximately 84/62 ppm), and ^{C}C4/6 (approximately 89/65 ppm), as indicated by the blue dash lines, in the high galactan sample compared to the control.

Pectin and xylan are not spatially close in the control secondary cell wall, and this is not enhanced by increasing galactan content

The distribution of pectin in the secondary cell wall is poorly understood, in part because of the low abundance. Here, we explored whether the pectin interacts with xylan and whether this is impacted by the extended galactan chains. 1D slices were extracted from DP-PDSD spectra with two relatively short mixing times (30 and 100 msec) at three xylan characteristic chemical shifts, ^{3f}Xn1 (102.5 ppm), ^{3f}Xn4 (77.4 ppm), and ^{3f}Xn5 (63.8 ppm) (Figure 4). These 1D slices show peaks at chemical shifts corresponding to the arabinosyl ($^{a–c}$A), galactosyl (^{a}Gal), and galacturonosyl (^{b}GalA) units from pectin, which indicates the presence of close proximities between three-fold screw xylan and pectin. For the short (30 msec) mixing time experiments, the spatial contacts between three-fold screw xylan and pectin were minor, with only a slight increase in the high galactan sample. This is unlike the spatial contacts between galactan and cellulose described above (Figure 3; Figure S14). In the longer mixing time experiment (100 msec), we detected stronger signals of spatial contacts between three-fold screw xylan and pectin in the high galactan sample only (Figure 4). This implies that the three-fold xylan is spatially distant from pectin as compared to cellulose.

Interestingly, there was a lack of cross peaks between units from pectin and the relatively rigid two-fold screw xylan observed in the short mixing time CP-PDSD experiments (as described in the following section) in either line (Figure 5). Two-fold screw xylan tightly binds to cellulose and contributes to mechanical strength in secondary cell walls (Busse-Wicher et al., 2014; Dupree et al., 2015; Grantham et al., 2017; Simmons et al., 2016), and these data imply that the additional galactan is not found in this region of the wall.

Increased crystalline cellulose is observed in the high galactan line

To further understand the effect of increasing galactan on the arrangement of cellulose, the short mixing time spectra of CP-PDSD of the wild-type and high galactan samples were overlaid in Figure 5a. The short mixing time (30 msec) allows comparison of the intramolecular contact cross peaks detected from both samples. The high galactan sample shows significantly increased intensities of cross peaks representing the intramolecular spatial contacts within the crystalline cellulose domain, as indicated in the blue box in Figure 5(a). Similarly, 1D slices were extracted from the vertical (F_1) dimension of CP-PDSD spectra of the wild-type and the high galactan samples respectively at five characteristic cellulose chemical shifts that represent C1 (105.2 ppm), ^{C}C4 (approximately 89 ppm), ^{A}C4 (approximately 84 ppm), ^{C}C6 (approximately 65 ppm), and ^{A}C6 (approximately 62 ppm) to better illustrate and compare the state of cellulose in both samples (Figure 5b). The CP-PDSD spectra with short mixing time (30 msec) were dominated by the intramolecular correlation of the rigid wall components, so the 1D slices extracted from ^{A}C6 and ^{C}C6 show mainly associations with ^{A}C1–5 and ^{C}C1–5, respectively, where ^{A}C6 shows dominant peaks at ^{A}C4 (approximately 84 ppm), ^{A}C2 (approximately 72.7 ppm), and ^{A}C3/5 (approximately 75 ppm) and ^{C}C6 shows dominant peaks at ^{C}C4 (approximately 89 ppm), ^{A}C2/5 (approximately 72.7 ppm), and ^{A}C3 (approximately 75 ppm) for both samples. However, the high galactan sample indicates a significant increase of all these intramolecular spatial contacts as compared to the wild-type sample, which implies a significantly increased abundance of cellulose in the high galactan secondary cell wall. Similar results are also observed in the 1D slices extracted for C1, ^{C}C4, and ^{A}C4. In addition, 1D slices at these characteristic chemical shifts of cellulose were extracted from CP-PDSD experiments with longer mixing times (100 and 1000 msec), and similar results are indicated by these spectra, as shown in Figure S15. To verify the changes to total cellulose content between the wild-type and the high galactan Arabidopsis basal stem material, the

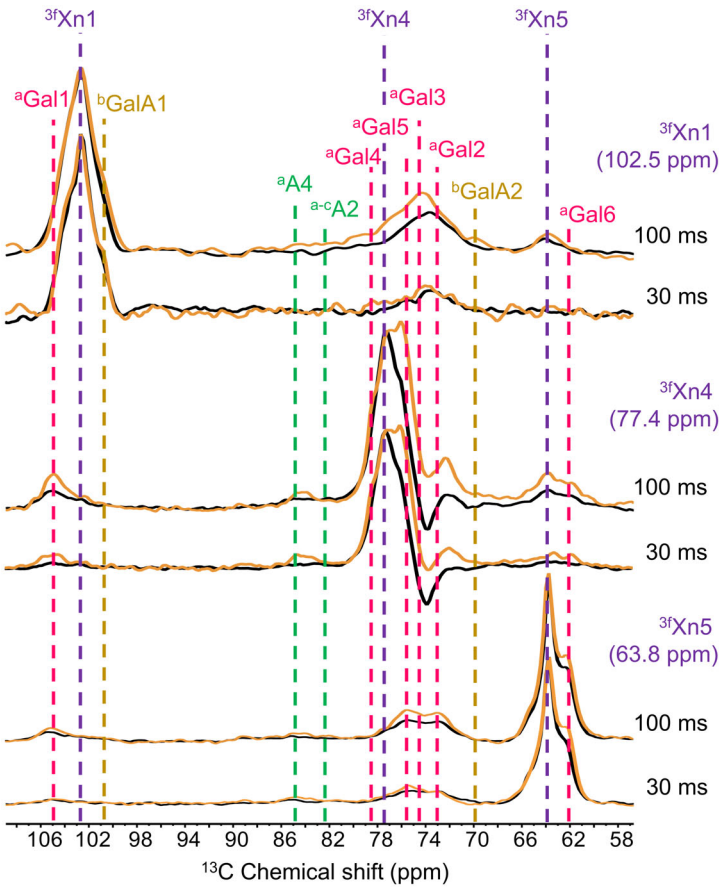

Figure 4. One-dimensional slices extracted from the direct polarization proton driven spin diffusion spectra (30 and 100 msec mixing times) F_2 dimensions at distinct three-fold screw xylan chemical shifts from the F_1 dimensions for the wild-type (black line) and high galactan samples (orange line).

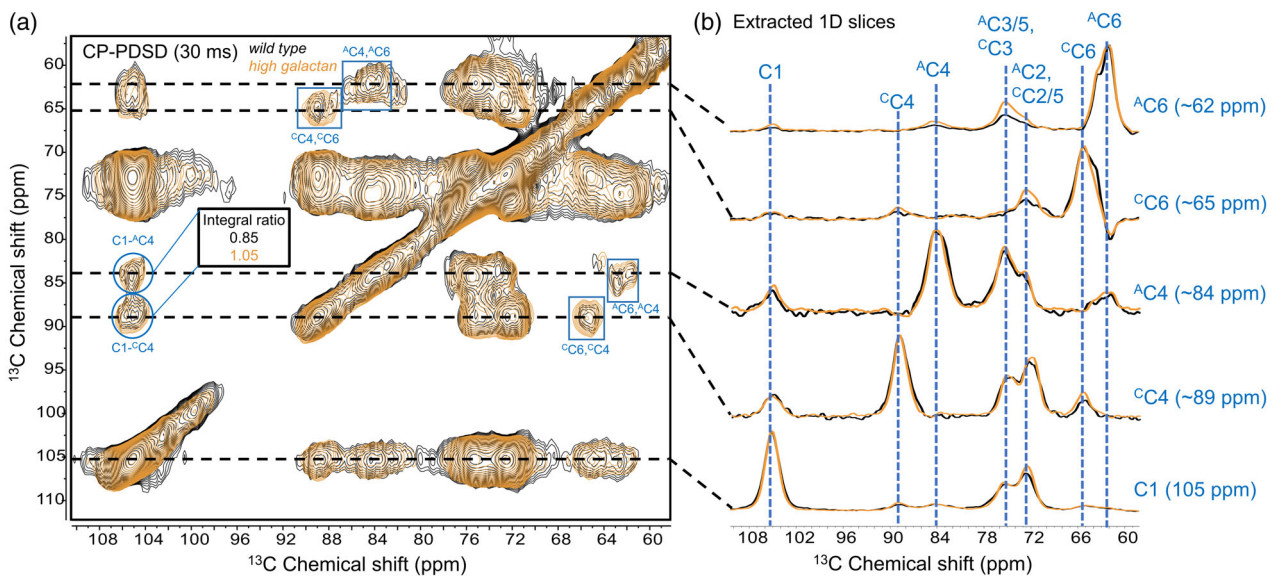

Figure 5. (a) An overlaid cross-polarization proton driven spin diffusion spectrum with short mixing time (30 msec) for the wild-type and high galactan samples. (b) One-dimensional slices were extracted at characteristic chemical shifts of cellulose at 105.2, approximately 89, approximately 84, approximately 65, and approximately 62 ppm.

monosaccharide composition in the cellulosic materials was obtained (Figure S16). However, there is no significant differences in cellulose content between the samples, which indicates that the enhanced galactan results in the deposition of more crystalline cellulose relative to amorphous cellulose, but not to an overall increase in cellulose content.

In the CP-PDSD spectra with short mixing time (30 msec), by assuming the cross peaks at (105.2 ppm, approximately 84 ppm) and (105.2 ppm, approximately 89 ppm) are only contributed by intramolecular spatial contacts between C1–^{A}C4 and C1–^{C}C4, respectively, we can estimate cellulose content by integration of these two cross peaks and obtain the ratio of amorphous to crystalline cellulose in both samples (Figure 5a). Results show that wild-type Arabidopsis has a crystalline-to-amorphous cellulose ratio of 0.85 (Terrett et al., 2019; Wang et al., 2016) and the transgenic Arabidopsis has a ratio of 1.05, which implies the high galactan plants have approximately 1.2 times more crystalline cellulose compared to amorphous cellulose than the control secondary cell wall-enriched material from wild type. Additionally, 1D magic angle spinning (MAS) ^{13}C CP experiments were performed and deconvoluted at the C4 region on both wild-type and high galactan samples to obtain their crystalline-to-amorphous cellulose ratios (Figure S17). These showed a similar increase in the high galactan sample, consistent with our CP-PDSD results.

DISCUSSION

Previously, multi-dimensional ssNMR has been used to develop a model of the nanoarchitecture of the Arabidopsis secondary cell wall containing the major components (cellulose, xylan, lignin) (Dupree et al., 2015; Gao et al., 2020; Kang et al., 2019; Terrett et al., 2019). However, it is less clear what role polysaccharides such as xyloglucan and pectin play, which are dominant in the primary cell wall but are minor components of the secondary cell wall (Moneo-Sánchez et al., 2019; Sandquist et al., 2010; Xiao & Anderson, 2013). In this study, we leverage a series of multi-dimensional ssNMR experiments to explore the effect of increased secondary cell wall-localized pectic galactan on the cell wall architecture.

In quantitative DP 1D ^{13}C NMR experiments, the high galactan secondary cell wall-enriched material shows a substantially increased overall abundance of polysaccharides relative to the wild type, particularly in the regions containing the chemical shifts of cellulose and pectin at approximately 105, 72–76, and 66–61 ppm. However, since the chemical shifts of galactan overlap with cellulose and many other polysaccharides in the 76–72 and 66–61 ppm regions, we employed 2D-INADEQUATE experiments to better resolve the chemical shifts from individual cell wall components. The DP-INADEQUATE shows significant enhancement of cross peaks from 1,4-linked galactosyl units (^{a}Gal) of galactan in the high galactan Arabidopsis, but not from the cross peaks from terminal galactosyl units (^{b}Gal). This observation suggests that the pectic galactan chains are elongated with more 1,4-linked galactosyl units in the high galactan sample, but the total number of galactan chains remains similar for both samples. This is consistent with our previous findings that the galactan biosynthesis enzyme GALS1 showed high activity with galactooligosaccharide acceptors and is capable of elongating β-1,4-galactans, but not initiating new galactan chains on the RG-I backbone (Ebert et al., 2018; Liwanag et al., 2012). This also verifies our assignments of the 1,4-linked and the terminal galactosyl units. Interestingly, despite the fact that GALS1 can act as a bifunctional enzyme and terminate galactan elongation by adding a terminal arabinosyl unit (Laursen et al., 2018), no increase of terminal arabinosyl units (^{a}A) was observed in the high galactan sample. This may be a result of substrate limitation, since UDP-Ara biosynthesis was not upregulated in these lines.

For the high galactan line, the enhancement of galactan was achieved by the co-expression of well-characterized genes, *GALS1*, *UGE2*, and *URGT1*, under the control of the secondary cell wall-specific *pC4H*, *pIRX5*, and *pIRX8* promoters, respectively (Aznar et al., 2018; Gondolf et al., 2014; Liwanag et al., 2012). We employed electron microscopic immuno-gold labeling with a pectic galactan monoclonal antibody (LM5) to confirm that galactan is significantly and specifically increased throughout the secondary cell walls of the high galactan plants, although the biological replicates of the high galactan line show some variation in labeling signal of LM5 epitopes (Figure 2d–f; Figures S3–S7). We believe it is reasonable to conclude that the vast majority of the elongated galactan chains in the high galactan plants are indeed present in the secondary cell wall, consistent with previously reported data (Aznar et al., 2018), although we cannot exclude the possibility that there are minor changes to the primary cell wall or middle lamella.

To investigate how the elongated galactan chains affect the spatial arrangement of other cell wall polysaccharides, we performed PDSD experiments with various mixing times. The DP-PDSD experiments showed significantly increased spatial contacts between the pectic backbone and galactan, as might be expected since galactan is a major side chain on the RG-I backbone. A recent simulation study on the 3D structure of RG-I indicates that its galactan side chains adopt conformations that are prone to intergalactan chain interactions (Makshakova et al., 2017), and therefore, it is likely that more of these associations are observed when galactan content is increased. For the same reasons, more contacts between galactan and arabinan were also observed in the DP-PDSD experiments

(Figure S14). In previous ssNMR studies on primary cell wall pectin, close proximities between pectin and cellulose were observed, and these were hypothesized to contribute to the mechanical properties of the cell wall (Dick-Pérez et al., 2011, 2012; Phyo et al., 2017; Wang & Hong, 2016; Wang, Park, et al., 2015). Although close spatial contacts between pectic galactan and cellulose were detected by ssNMR (Figure 3; Figures S14 and S18), because of the high mobility of these polysaccharides, researchers believed these contacts were via the pectic backbone GalA units (Phyo et al., 2017; Wang & Hong, 2016). Our CP-PDSD experiments on the wild-type secondary cell wall-enriched material indicate similar results, with close proximities between the galacturonosyl units from the backbone and cellulose (Figure 3; Figure S18). Interestingly, there is a major reduction of such contacts in the high galactan Arabidopsis line. Instead, close proximities between pectic galactan and cellulose were also observed by the CP-PDSD experiments (Figure 3). We interpret these data as showing that a fraction of the elongated galactan is also closely and rigidly associated with cellulose, and as a result blocks cellulose–pectic backbone interactions. Zykwinska et al. (2005, 2008) have reported that pectin interacts with cellulose through its side chains instead of through its backbone. The observed enhancement of 1,4-linked galactosyl units and unchanged arabinosyl units indicate that the elongated galactan chains in the high galactan Arabidopsis may suffer from less steric hindrance from arabinan branches, and therefore have an increased potential for interaction with cellulose. However, our INADEQUATE data (Figure 2; Figure S14) also indicate that a large fraction of the galactan chains remains relatively mobile, despite the increased association with with cellulose. Zykwinska et al. also indicated that the interactions between pectic side chains and cellulose were likely mediated by hydrogen bonds, but pectic side chains bound less efficiently with cellulose (compared to polysaccharides that have a flat ribbon shape, for example two-fold screw xylan and xyloglucan) due to the conformational anisotropy of pectic side chains, which contrasts with the two-fold ribbon conformation of cellulose (Zykwinska et al., 2005). Furthermore, *in vivo* studies of interactions between pectic side chains and cellulose showed that cellulose-bound pectic side chains demonstrated a high mobility and that these interactions are reversible (Lin et al., 2015). Hence, the reduced hydrogen-bonding capacity between galactan and cellulose, as compared to that between two-fold screw xylan and cellulose, may induce reversible binding and preserve the high mobility of a great fraction of the elongated galactan, even when spatially close to cellulose.

Another notable change in the cell walls of the high galactan Arabidopsis is that much less xyloglucan was detected in both CP- and DP-INADEQUATE experiments compared to the wild-type control. Consequently, in the high galactan Arabidopsis, fewer spatial contacts between xyloglucan and cellulose were detected by PDSD experiments with short mixing times. In particular, the CP-PDSD with a mixing time of 30 msec showed that substantially less xyloglucan was entrapped in the cellulose microfibrils. This is consistent with a recent study by Moneo-Sanchez et al., which found that pectic galactan could directly compete with xyloglucan in binding cellulose during elongation, and less galactan leads to more access of xyloglucan to cellulose microfibrils (Moneo-Sánchez et al., 2019). This could be due to increased competition for UDP-Glc as a result of the strategy used to increase galactan content. Here, we overexpressed a cytosolic UGE to increase the availability of UDP-Gal for galactan biosynthesis, and it is possible that less UDP-Glc is available for interconversion into nucleotide sugars required for xyloglucan biosynthesis, such as UDP-Xyl (Feingold, 1982; Tenhaken & Thulke, 1996). Although xyloglucan is not the major hemicellulose in the secondary cell wall, it is still an important wall component that is believed to serve a load-bearing role for microfibrils (Hayashi & Kaida, 2011; Moneo-Sánchez et al., 2019). Moneo-Sanchez et al. also reported that decreased pectic galactan content could lead to more xyloglucan–cellulose interactions during secondary cell wall deposition, indicating that the competition between galactan and xyloglucan for binding cellulose is maintained after the cessation of cell elongation (Moneo-Sánchez et al., 2020). This further supports our observations in the high galactan Arabidopsis secondary cell walls. However, the reduced xyloglucan–cellulose spatial contacts may also be due to the reduction of total xyloglucan content in the high galactan line.

A series of ssNMR (Dick-Pérez et al., 2011, 2012; Phyo et al., 2017; Wang & Hong, 2016; Wang, Park, et al., 2015) and biochemistry (Lin et al., 2015; McCartney et al., 2000; Moneo-Sánchez et al., 2019; Zykwinska et al., 2007; Zykwinska et al., 2008) studies have shown that, in the primary cell wall, pectin closely interacts with both cellulose and xyloglucan and critically contributes to the wall mechanical properties. In the secondary cell wall, instead of xyloglucan, xylan is the major hemicellulose. Hence, understanding how pectin interacts with xylan is crucial to interpreting the role of pectin in the mechanical properties of the secondary cell wall. Our DP-PDSD experiments indicated that spatial contacts between xylan and pectin exist in Arabidopsis secondary cell wall-enriched material. Since enhanced pectin–cellulose contacts were detected in the high galactan sample in the 30 msec mixing time experiment, this implies that pectin and three-fold screw xylan have greater spatial separation than pectin and cellulose. In addition, few spatial contacts were observed between two-fold screw xylan and pectin in our PDSD experiments with short mixing times, which indicates that pectin interacts more with the mobile fraction of xylan in the three-

fold screw conformation. Hence, we hypothesize that even though pectin interacts with both xylan and cellulose, due to the highly mobile nature of these contacts, the role of pectin in the mechanical properties of the secondary cell wall is less significant than in those of the primary cell wall. Instead, as one of the three major components, lignin may play a bigger role in the mechanical properties of secondary cell walls (Kang et al., 2019). Further studies on changes of lignin interactions in engineered Arabidopsis secondary cell walls are needed to better elucidate its role.

Finally, our PDSD experiments with a short mixing time (30 msec), which are dominated by intramolecular contacts, show enhanced cross peaks between cellulose within each domain (i.e., crystalline or amorphous) in the high galactan Arabidopsis. The ratio of crystalline to amorphous cellulose also increased from 0.85 in the wild-type to 1.05 in the high galactan Arabidopsis. This has parallels to the cell wall changes described for tension wood, a specialized form of secondary cell wall which forms in woody stems in response to bending stress as a corrective growth process (Gorshkova et al., 2015; Sawada et al., 2018). Tension wood contains a thick structure called the gelatinous layer (G-layer). As secondary wall development proceeds, a thickened galactan-rich matrix is newly deposited (Gorshkova et al., 2004; Gorshkova et al., 2015; Roach et al., 2011). The G-layer is lower in xylan and lignin than normal secondary cell walls, but rich in cellulose microfibrils which have large regions of crystallinity (Roach et al., 2011). It is possible that similar processes drive the increased cellulose crystallinity in tension wood as we observed in our high galactan Arabidopsis.

Our multi-dimensional ssNMR analysis of engineered Arabidopsis has allowed us to test and revise the model of the secondary cell wall (Figure 6). In wild-type Arabidopsis, in addition to two-fold screw xylan, both the pectic backbone and xyloglucan directly bind cellulose microfibrils to contribute to the mechanical properties of the cell wall (Dick-Pérez et al., 2011, 2012; Phyo et al., 2017; Wang & Hong, 2016; Wang, Park, et al., 2015). Pectic side chains could also closely interact with cellulose, but the nature of such interactions is relatively mobile. However, when the pectic galactan was highly expressed in the high galactan Arabidopsis, the long pectic galactan chains can lead to inefficient binding with cellulose due to its non-ribbon conformation. The pectic galactan chains can also associate with each other and block the binding site and prevent the pectic backbone and xyloglucan from binding with cellulose, which leads to a loosened secondary cell wall architecture (Dick-Pérez et al., 2011, 2012; Kirui et al., 2021; Wang et al., 2012; Wang, Park, et al., 2015). This may explain previous results by Yan et al., who conducted a saccharification assay which showed that increased cell wall galactan content improved release of hexose even

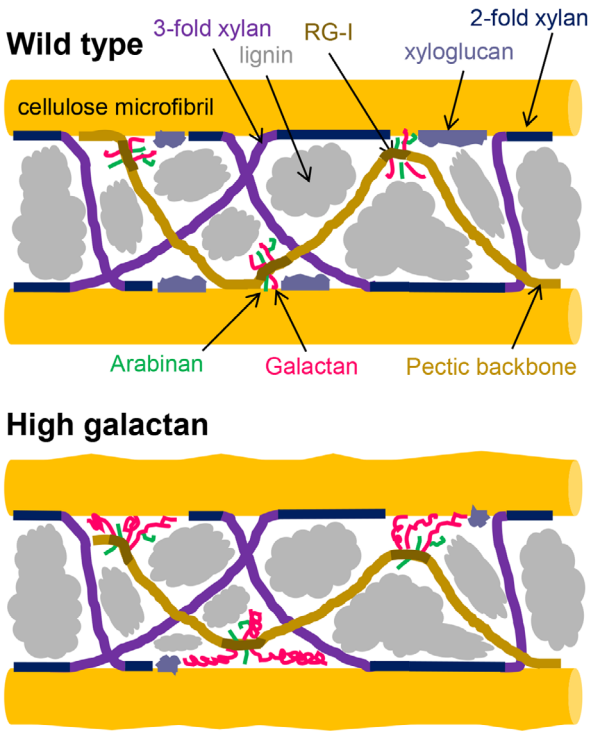

Figure 6. Models of secondary cell wall architecture of wild-type and high galactan Arabidopsis with elongated pectic galactan chains.

without addition of galactanase to the cell wall-degrading enzyme cocktail (Yan et al., 2018).

There is also a possibility that some of the enhanced galactan signals are contributed by the presence of free galactan chains in the cell wall, cleaved from the RG-I polymer by cell wall remodeling enzymes. We were unable to show direct evidence of covalent links between galactan and the RG-I backbone by ssNMR. Our previous studies of *GALS1*-overexpressing plants have demonstrated that elongated galactan chains are isolated together with RG-I after pectinase treatment and size-exclusion chromatography, suggesting that any free galactan is a minor component (Ebert et al., 2018; Laursen et al., 2018). However, if free galactan is present in the secondary walls, it may still disrupt 'normal' RG-I backbone associations within pectin, which would lead to similar observations in some of the ssNMR data. We see a clear partitioning in our data, where the increased galactan is more closely associated with cellulose and the pectic backbone but relatively distanced from the xylan. This is consistent with most of the galactan being found as side chains in RG-I, where free galactan might be expected to be more evenly distributed within the cell wall nanoarchitecture and also associate with, for example, xylan. Although we cannot exclude the presence of galactan unattached to RG-I, we think it is reasonable to conclude that it is likely a minor portion of the enhanced

galactan content and propose a cell wall model accordingly (Figure 6). Future work making use of additional lines of engineered plants with altered cell walls would be useful to test this further.

Interestingly, it has also been recently reported that RG-I pectin plays a critical role in cell–cell adhesion in poplar stems (Yang et al., 2020), via potential cross-links with xylan and lignin in the middle lamella. In turn, this loss of cell–cell adhesion is also able to enhance saccharification by loosening the cellular structure, allowing better penetration of cell wall-degrading enzymes. In our experiments, since we used intact plant stems, primary cell wall and middle lamella were necessarily also included. By using basal stem material, the tissue is highly enriched in secondary cell walls, as demonstrated by the lignin and monosaccharide composition. Therefore, although there are signals derived from the primary cell wall and middle lamella in our spectra, we have taken every effort to minimize them. Since our plants only express the gene encoding the galactan-elongating enzyme under the control of a secondary cell wall-specific promoter, we were not able to test the effects of pectic galactan elongation on these other cell wall types. However, by developing similar high galactan lines using primary cell wall-specific promoters, along with constitutive promoters, it will be interesting to compare the effects on both saccharification and cell wall organization. Finally, advances in gene editing which now allow cell-specific targeting of enzymes (Liang et al., 2019) will enable testing the effects of cell wall engineering on specific cell types, which will certainly enhance our understanding of these systems.

To conclude, in this study, we employed multidimensional ssNMR to reveal the native structural environment of the secondary cell wall architecture of wild-type and engineered Arabidopsis with high galactan content. By modifying the cell wall composition and investigating the impact on the wall architecture, we were able to better understand the role of pectic galactan in the secondary cell wall. This engineering approach successfully increased the galactan content in the secondary cell wall and enhanced the hexose-to-pentose ratio. In the engineered plants pectic galactan closely associates with cellulose, and the elongated galactan chains block binding sites of cellulose for xyloglucan and the pectic backbone. This results in a loosened secondary cell wall architecture. A loosened wall architecture promotes decomposition of the biomass, but our results suggest that the introduction of this strategy into woody biomass or other bioenergy crops would benefit from cell-specific expression to avoid negative effects on plant growth. Finally, we also demonstrate how methods such as ssNMR can be used in the context of synthetic biology to learn from engineering strategies and to refine future approaches.

EXPERIMENTAL PROCEDURES

Plant materials

The wild-type and high galactan Arabidopsis (*A. thaliana* (L.) Heynh.) lines used in this work were both ecotype Columbia-0. The high galactan line used (W2-4) was previously described (Aznar et al., 2018) and was generated by expressing *GALS1*, *UGE2*, and *URGT1* under the control of the secondary cell wall-specific *pC4H*, *pIRX5*, and *pIRX8* promoters, respectively.

Generation of ^{13}C-enriched plant materials

Arabidopsis seeds were surface sterilized and sown on half strength Murashige and Skoog agar plates with 0.7% (w/v) agar and 1% (w/v) sucrose. Seeds were stratified for 48 h at 4°C under dark conditions and then transferred to a growth chamber (23°C, 150 μmol m^{-2} sec^{-1}, 15/9 h light/dark photoperiod) to germinate vertically for 10 days. Then, 10 wild-type and 10 high galactan seedlings were transferred to two hydroponic containers (five of each per container) and placed into a self-constructed growth chamber (24°C, 60% humidity, 155 μmol m^{-2} sec^{-1}, 18/6 h light/dark photoperiod) with a controlled $^{13}CO_2$ atmosphere as previously described in Gao and Mortimer (2020). Plants were grown for an additional 29 days. At harvest, plant material was dissected into three general types of tissue, including stem, leaves, and roots, snap frozen in liquid nitrogen, and stored at −80°C for later analysis. A subsample of leaf tissue was used to calculate the ^{13}C incorporation of the Arabidopsis plants by the procedure described in Atalla and Vanderhart (1984, 1999) and Gao et al. (2020). The ^{13}C incorporation of Arabidopsis plants used in this study was >90%. Tissue from the lower one third of the main stem, which is highly enriched in the secondary cell wall, was collected from both the wild-type (control) and the high galactan Arabidopsis. Stem tissue was sliced into 1–2-mm pieces and directly packed into a 3.2-mm rotor without further processing to preserve the native arrangement of wall components.

Immuno-gold labeling and TEM

Base stems at growth stage 6.9 (Boyes et al., 2001) were chemically fixed, dehydrated, and embedded in LR white according to the method outlined in Wilson and Bacic (2012). Thin sections (approximately 80 nm) were acquired for antibody labeling and post-stained (Wilson & Bacic, 2012). For antibody labeling, samples were incubated with LM5 (1,4-β-D-galactan) monoclonal antibodies (source: rat) (Jones et al., 1997) or CCRC-M35 (RG-I) monoclonal antibodies (source: mouse) (Pattathil et al., 2010) at 1:20 dilution for 2 h at room temperature. Samples were then washed and incubated with goat anti-rat 18 nm gold-conjugated secondary antibody (Jackson Immuno Research, West Grove, PA, USA; #112–215-167) or goat anti-mouse 18 nm gold-conjugated secondary antibody (Jackson Immuno Research; #115–215-166) at 1:20 dilution for 1 h at room temperature. Detection of 1,4-β-D-galactan was performed on two biological replicates. Grids were imaged using a Jeol (Tokyo, Japan) 2100 electron microscope equipped with a Gatan (Pleasanton, CA, USA) Orius SC 200 CCD camera.

For quantification of gold particles/area, the total cell wall area (primary cell wall/middle lamella and secondary wall) on a TEM image was determined using ImageJ and gold particles within the wall were counted. The number of gold particles per μm^2 of wall was then calculated for 3–10 cells for each biological replicate.

Magic angle spinning ssNMR

All MAS ssNMR experiments in this work were performed on an Agilent (Santa Clara, CA, USA) 850 WB with a direct drive (VNMRS) NMR console operating at 20.0 T, corresponding to ^{1}H and ^{13}C Larmor frequencies of 849.727 and 213.685 MHz, using an Agilent 3.2 mm HXY MAS probe tuned in double resonance mode. Never-dried plant tissue samples were sliced and directly packed into 3.2-mm zirconia rotors with o-ring seals (Revolution NMR, Fort Collins, CO, USA). The total weights of the packed rotors were tracked to ensure negligible loss of water from the plant materials during ssNMR experiments. All experiments were conducted at room temperature with a MAS frequency of 13 kHz. The 1D ^{13}C MAS NMR was conducted with DP and a long recycle delay (30 sec) to yield quantitative intensities and a total of 256 transients were acquired. The 2D DQ to SQ ^{13}C–^{13}C correlation experiments, which use scalar *J* coupling to detect directly coupled nuclei through bonds, were performed via a refocused INADEQUATE (Lesage et al., 1997, 2000) pulse sequence with either DP or CP. Experiments with CP were performed with a standard ramped CP pulse sequence using a 4 μsec ^{1}H 90° pulse, a 1 msec contact pulse (ramped ^{1}H RF amplitude; Metz et al., 1994), and a 2 sec recycle delay. SPINAL-64 decoupling (Fung et al., 2000) was applied during acquisition at a ^{1}H nutation frequency of 62–80 kHz. The 2D PDSD (Takegoshi et al., 2001; Wang, Williams, et al., 2015) ^{13}C–^{13}C correlation experiments, which are based on distance-dependent dipolar coupling to detect coupled nuclei through space, were performed with either DP or CP at a series of mixing times (30, 100, and 1000 msec). The relaxation-compensated PDSD ^{13}C–^{13}C correlation experiments (Wang, Williams, et al., 2015) were performed at room temperature using a constant z-period of 1.05 sec with two different mixing times (200 and 1000 msec). The ^{13}C chemical shifts are referenced relative to tetramethylsilane ($(CH_3)_4Si$) by assignment of the methylene peak in adamantane at 38.48 ppm as an external secondary standard. The data obtained were Fourier transformed into 2 K (F_2) × 1 K (F_1) points with EM line broadening of 100 Hz in F_2 and squared sine bell in F_1. All NMR data were processed with software MestreNOVA (v. 14). The assignments of the wall components in this work were referenced to published literature and provided in Table S1 in the supplementary information.

Cell wall monosaccharide composition analysis of the ^{13}C plant materials

Stem tissue samples from the ^{13}C-enriched Arabidopsis were first processed into alcohol-insoluble residue (AIR) as described in Gao and Mortimer (2020). The AIR samples (1 mg) were hydrolyzed with fresh 2 M trifluoroacetic acid at 120°C for 1 h. The hydrolyzed AIR supernatants were retained, dried in a vacuum concentrator, and redissolved in 1 ml of Millipore water. Samples were diluted 50 times and filtered through 0.22-μm filters for high performance anion exchange chromatography equipped with pulsed amperometric detection (HPAEC-PAD) analysis. The leftover solid residues were dried and then hydrolyzed with 72% sulfuric acid at room temperature for 1 h. The concentration of sulfuric acid in the samples were then diluted to 1 M, and the samples were incubated at 100°C for 3 h. The hydrolyzed supernatants were retained, neutralized with barium sulfate, and dried with a vacuum concentrator. The obtained monosaccharides were redissolved in 1 ml of Millipore water, diluted 100-fold with water, and then filtered through 0.22-μm filters for HPAEC-PAD analysis.

Samples were injected into a Dionex ICS-5000 instrument (Thermo Fisher Scientific) equipped with a CarboPac PA20 analytical anion exchange column (3 mm × 150 mm; Thermo Fisher Scientific), a PA20 guard column (3 mm × 30 mm; Thermo Fisher Scientific), a borate trap, and a pulsed amperometric detector. The column was equilibrated with 40 mM NaOH for 5 min. Monosaccharides were separated by using a linear gradient from 4 mM NaOH to 3 mM NaOH in the first 6 min, followed by a linear gradient of 3 mM NaOH to 1 mM NaOH from 6 to 8 min. An isocratic gradient was held at 1 mM NaOH from 8 to 23 min. The gradient was then increased to 450 mM NaOH to elute the acidic sugar from 23.1 to 45 min.

Klason lignin analysis

The Klason method was performed to determine the acid-insoluble lignin content of pooled stem tissue from six biological replicates for both wild-type and high galactan samples according to the NREL protocol (NREL/TP-510-42 618; Sluiter et al., 2008).

ACKNOWLEDGMENTS

We thank Dr. Christopher Gee for taking the time to teach us the preparation and slicing of sample blocks for imaging. We thank Dr. Nancy M. Washton and Dr. Sarah D. Burton, Environmental Molecular Sciences Laboratory, for help with coordinating and set-up of the ssNMR experiments. This work was conducted as part of the DOE Joint BioEnergy Institute (http://www.jbei.org) supported by the U.S. Department of Energy, Office of Science, Office of Biological and Environmental Research, through contract DE-AC02-05CH11231 between Lawrence Berkeley National Laboratory and the U.S. Department of Energy (JCM, HVS, YG). A portion of this research was performed on awards (DOI: 10.46936/sarr.proj.2018.50159/60006349 and 10.46936/lser.proj.2020.51332/60000172) from the Environmental Molecular Sciences Laboratory, a DOE Office of Science User Facility sponsored by the Biological and Environmental Research program under Contract No. DE-AC05-76RL01830 (ASL, JCM, YG, DTM). The work was also supported by startup funding from the University of California, Davis (DTM) and the University of Adelaide (JCM). Open access publishing facilitated by The University of Adelaide, as part of the Wiley - The University of Adelaide agreement via the Council of Australian University Librarians.

CONFLICT OF INTEREST

The authors have not declared a conflict of interest.

DATA AVAILABILITY STATEMENT

All underlying data described in this manuscript are available either in the supplementary material or in the EMSL data repository (NEXUS) (https://doi.org/10.25582/data.2023-03.2769303/1961836).

SUPPORTING INFORMATION

Additional Supporting Information may be found in the online version of this article.

Figure S1. Monosaccharide composition of non-cellulosic polysaccharides in mature Arabidopsis stem AIR.

Figure S2. Overlaid DP-INADEQUATE spectra of the wild-type (black) and the high galactan (orange) Arabidopsis stem material at regions (SQ: 87–60 ppm and DQ: 164–132 ppm) which better demonstrate two distinct sets of signals from galactosyl units from galactan labeled as ^{a,b}Gal2-6 that represent 1,4-linked and terminal units, respectively.

Figure S3. TEM immuno-gold labeling detection of pectic 1,4-β-D-galactan with LM5 antibody in walls of interfascicular fiber, xylem vessel, and parenchyma cells in transverse sections at 1 cm from the stem base of stage 6.9 (Boyes et al., 2001) wild-type Arabidopsis replicate 1. Scale bar = 1 μm.

Figure S4. TEM immuno-gold labeling detection of pectic 1,4-β-D-galactan with LM5 antibody in walls of interfascicular fiber, xylem vessel, and parenchyma cells in transverse sections at 1 cm from the stem base of stage 6.9 (Boyes et al., 2001) wild-type Arabidopsis replicate 2. Scale bar = 1 μm.

Figure S5. TEM immuno-gold labeling detection of pectic 1,4-β-D-galactan with LM5 antibody in walls of interfascicular fiber, xylem vessel, and parenchyma cells in transverse sections at 1 cm from the stem base of stage 6.9 (Boyes et al., 2001) high galactan Arabidopsis replicate 1. Scale bar = 1 μm.

Figure S6. TEM immuno-gold labeling detection of pectic 1,4-β-D-galactan with LM5 antibody in walls of interfascicular fiber, xylem vessel, and parenchyma cells in transverse sections at 1 cm from the stem base of stage 6.9 (Boyes et al., 2001) high galactan Arabidopsis replicate 2. Scale bar = 1 μm.

Figure S7. TEM immuno-gold labeling detection control with no primary LM5 antibody in walls of interfascicular fiber, xylem vessel, and parenchyma cells in transverse sections at 1 cm from the stem base of stage 6.9 (Boyes et al., 2001) wild-type Arabidopsis. Scale bar = 1 μm.

Figure S8. Location of pectin in interfascicular fiber cells at the base region of stems.

Figure S9. TEM immuno-gold labeling detection of RG-I with CCRC-M35 antibody in walls of interfascicular fiber, xylem vessel, and parenchyma cells in transverse sections at 1 cm from the stem base of stage 6.9 (Boyes et al., 2001) wild-type Arabidopsis replicate 1. Scale bar = 1 μm.

Figure S10. TEM immuno-gold labeling detection of RG-I with CCRC-M35 antibody in walls of interfascicular fiber, xylem vessel, and parenchyma cells in transverse sections at 1 cm from the stem base of stage 6.9 (Boyes et al., 2001) wild-type Arabidopsis replicate 3. Scale bar = 1 μm.

Figure S11. TEM immuno-gold labeling detection of rhamnogalacturonan-I with CCRC-M35 antibody in walls of interfascicular fiber, xylem vessel, and parenchyma cells in transverse sections at 1 cm from the stem base of stage 6.9 (Boyes et al., 2001) high galactan Arabidopsis replicate 3. Scale bar = 1 μm.

Figure S12. Overlaid DP-INADEQUATE spectra of the wild-type (black) and the high galactan (orange) Arabidopsis stem material at the major polysaccharide region. This is an enlargement of Figure 2(a) in the main text.

Figure S13. Overlaid CP-INADEQUATE spectra of the wild-type (black) and the high galactan (orange) Arabidopsis stem material at the major polysaccharide region.

Figure S14. (a) An overlaid DP-PDSD spectrum with short mixing time (30 msec) and short recycle delay (2 sec) shows spatial contacts between spatially close mobile carbons. (b) 1D slices extracted from the F_2 dimensions at seven chemical shifts from the F_1 dimensions of the DP-PDSD spectra of the wild-type and the high galactan samples. Inset is the zoom-in window, better showing the characteristic cellulose C4 region of the three extracted 1D slices from Gal2, Gal3, and Gal5 between the wild-type and the high galactan samples.

Figure S15. An overlaid CP-PDSD spectrum with relatively long mixing times (100, 1000 msec) for the wild-type and the high galactan samples. 1D slices were extracted at characteristic chemical shifts of cellulose at 105.2, approximately 89, approximately 84, approximately 65, and approximately 62 ppm.

Figure S16. Monosaccharide composition analysis of cellulosic materials in the cell walls from stem tissue of both wild-type and high galactan ^{13}C Arabidopsis. Monosaccharide quantities are the average values of five biological replicates. The error bars are standard deviations.

Figure S17. (a) 1D MAS ^{13}C CP experiments on the stem tissue of wild-type and high galactan Arabidopsis (spectra were normalized at the crystalline cellulose C4 region, approximately 89 ppm). (b) Spectra were deconvoluted and integrated by a built-in Global Spectral Deconvolution (GSD) method in MestReNova NMR processing software (Version 14.1.0). The crystalline-to-amorphous cellulose ratio is determined as 0.94 for the wild-type and 1.16 for the high galactan Arabidopsis.

Figure S18. Overlaid T1-compensated PDSD difference spectra of the wild-type and high galactan samples.

Figure S19. An overlaid CP-PDSD spectrum with short mixing time (30 msec), which shows relatively short distance contacts between relatively rigid wall components, for the wild-type (black line) and the high galactan (orange line) stem samples. Close proximities between C4 and C6 from both crystalline and amorphous cellulose domains are indicated in blue boxes.

Figure S20. (a) ^{13}C T_1 measurement from both domains of cellulose and galactan. (b) The fraction of the long T1 component. Data are presented as mean value ± standard error of the mean (SEM). Error bars are SEM values of the fitting parameters on 25 data points. Data were fitted with a biexponential function.

Table S1. Comparison of the Klason lignin content between the Arabidopsis tissue used for this study and other published data on wild-type Arabidopsis.

Table S2. Chemical shift assignment of the cell wall components.

REFERENCES

Atalla, R.H. & **Vanderhart, D.L.** (1984) Native cellulose: a composite of two distinct crystalline forms. *Science*, **223**, 283–285.

Atalla, R.H. & **Vanderhart, D.L.** (1999) The role of solid state ^{13}C NMR spectroscopy in studies of the nature of native celluloses. *Solid State Nuclear Magnetic Resonance*, **15**, 1–19.

Aznar, A., Chalvin, C., Shih, P.M., Maimann, M., Ebert, B., Birdseye, D.S. *et al.* (2018) Gene stacking of multiple traits for high yield of fermentable sugars in plant biomass. *Biotechnology for Biofuels*, **11**, 2.

Boyes, D.C., Zayed, A.M., Ascenzi, R., McCaskill, A.J., Hoffman, N.E., Davis, K.R. *et al.* (2001) Growth stage-based phenotypic analysis of Arabidopsis: a model for high throughput functional genomics in plants. *Plant Cell*, **13**, 1499–1510.

Bromley, J.R., Busse-Wicher, M., Tryfona, T., Mortimer, J.C., Zhang, Z., Brown, D.M. *et al.* (2013) GUX1 and GUX2 glucuronyltransferases decorate distinct domains of glucuronoxylan with different substitution patterns. *The Plant Journal*, **74**, 423–434.

Busse-Wicher, M., Gomes, T.C.F., Tryfona, T., Nikolovski, N., Stott, K., Grantham, N.J. *et al.* (2014) The pattern of xylan acetylation suggests xylan may interact with cellulose microfibrils as a twofold helical screw in the secondary plant cell wall of *Arabidopsis thaliana*. *The Plant Journal*, **79**, 492–506.

Caffall, K.H. & **Mohnen, D.** (2009) The structure, function, and biosynthesis of plant cell wall pectic polysaccharides. *Carbohydrate Research*, **344**, 1879–1900.

Dick-Pérez, M., Wang, T., Salazar, A., Zabotina, O.A. & **Hong, M.** (2012) Multidimensional solid-state NMR studies of the structure and dynamics of pectic polysaccharides in uniformly ^{13}C-labeled Arabidopsis primary cell walls. *Magnetic Resonance in Chemistry*, **50**, 539–550.

Dick-Pérez, M., Zhang, Y., Hayes, J., Salazar, A., Zabotina, O.A. & **Hong, M.** (2011) Structure and interactions of plant cell-wall polysaccharides by

two- and three-dimensional magic-angle-spinning solid-state NMR. *Biochemistry*, **50**, 989–1000.

Dupree, R., Simmons, T.J., Mortimer, J.C., Patel, D., Iuga, D., Brown, S.P. *et al.* (2015) Probing the molecular architecture of *Arabidopsis thaliana* secondary cell walls using two- and three-dimensional (13)C solid state nuclear magnetic resonance spectroscopy. *Biochemistry*, **54**, 2335–2345.

Ebert, B., Birdseye, D., Liwanag, A.J.M., Laursen, T., Rennie, E.A., Guo, X. *et al.* (2018) The three members of the Arabidopsis glycosyltransferase family 92 are functional β-1,4-galactan synthases. *Plant & Cell Physiology*, **59**, 2624–2636.

Eudes, A., Sathitsuksanoh, N., Baidoo, E.E.K., George, A., Liang, Y., Yang, F. *et al.* (2015) Expression of a bacterial 3-dehydroshikimate dehydratase reduces lignin content and improves biomass saccharification efficiency. *Plant Biotechnology Journal*, **13**, 1241–1250.

Feingold, D.S. (1982) Aldo (and keto) hexoses and uronic acids. In: Loewus, F.A. & Tanner, W. (Eds.) *Plant carbohydrates I*. Berlin, Heidelberg: Springer Berlin Heidelberg, pp. 3–76.

Fung, B.M., Khitrin, A.K. & Ermolaev, K. (2000) An improved broadband decoupling sequence for liquid crystals and solids. *Journal of Magnetic Resonance*, **142**, 97–101.

Gao, Y., Beganovic, M. & Foston, M.B. (2016) Lignin conversion to fuels and chemicals. In: Kumar R, Singh S, Balan V, eds. *Valorization of lignocellulosic biomass in a biorefinery: from logistics to environmental and performance impact*. Hauppauge, NY: Nova Science Publishers, pp. 245–292.

Gao, Y., Lipton, A.S., Wittmer, Y., Murray, D.T. & Mortimer, J.C. (2020) A grass-specific cellulose-xylan interaction dominates in sorghum secondary cell walls. *Nature Communications*, **11**, 6081.

Gao, Y. & Mortimer, J.C. (2020) Unlocking the architecture of native plant cell walls via solid-state nuclear magnetic resonance. *Methods in Cell Biology*, **160**, 121–143.

Gondolf, V.M., Stoppel, R., Ebert, B., Rautengarten, C., Liwanag, A.J., Loqué, D. *et al.* (2014) A gene stacking approach leads to engineered plants with highly increased galactan levels in Arabidopsis. *BMC Plant Biology*, **14**, 344.

Gorshkova, T., Mokshina, N., Chernova, T., Ibragimova, N., Salnikov, V., Mikshina, P. *et al.* (2015) Aspen tension wood fibers contain β-(1→4)-galactans and acidic arabinogalactans retained by cellulose microfibrils in gelatinous walls. *Plant Physiology*, **169**, 2048–2063.

Gorshkova, T.A., Chemikosova, S.B., Sal'nikov, V.V., Pavlencheva, N.V., Gur'janov, O.P., Stolle-Smits, T. *et al.* (2004) Occurrence of cell-specific galactan is coinciding with bast fiber developmental transition in flax. *Industrial Crops and Products*, **19**, 217–224.

Grantham, N.J., Wurman-Rodrich, J., Terrett, O.M., Lyczakowski, J.J., Stott, K., Iuga, D. *et al.* (2017) An even pattern of xylan substitution is critical for interaction with cellulose in plant cell walls. *Nature Plants*, **3**, 859–865.

Hao, Z., Yogiswara, S., Wei, T., Benites, V.T., Sinha, A., Wang, G. *et al.* (2021) Expression of a bacterial 3-dehydroshikimate dehydratase (QsuB) reduces lignin and improves biomass saccharification efficiency in switchgrass (*Panicum virgatum* L.). *BMC Plant Biology*, **21**, 56.

Hayashi, T. & Kaida, R. (2011) Functions of xyloglucan in plant cells. *Molecular Plant*, **4**, 17–24.

Jones, L., Seymour, G.B. & Knox, J.P. (1997) Localization of pectic galactan in tomato cell walls using a monoclonal antibody specific to (1[→]4)-[beta]-D-galactan. *Plant Physiology*, **113**, 1405–1412.

Kang, X., Kirui, A., Dickwella Widanage, M.C., Mentink-Vigier, F., Cosgrove, D.J. & Wang, T. (2019) Lignin-polysaccharide interactions in plant secondary cell walls revealed by solid-state NMR. *Nature Communications*, **10**, 347.

Kirui, A., Du, J., Zhao, W., Barnes, W., Kang, X., Anderson, C.T. *et al.* (2021) A pectin methyltransferase modulates polysaccharide dynamics and interactions in Arabidopsis primary cell walls: evidence from solid-state NMR. *Carbohydrate Polymers*, **270**, 118370.

Larsen, F.H., Byg, I., Damager, I., Diaz, J., Engelsen, S.B. & Ulvskov, P. (2011) Residue specific hydration of primary cell wall potato pectin identified by solid-state ^{13}C single-pulse MAS and CP/MAS NMR spectroscopy. *Biomacromolecules*, **12**, 1844–1850.

Laursen, T., Stonebloom, S.H., Pidatala, V.R., Birdseye, D.S., Clausen, M.H., Mortimer, J.C. *et al.* (2018) Bifunctional glycosyltransferases catalyze both extension and termination of pectic galactan oligosaccharides. *The Plant Journal*, **94**, 340–351.

Lesage, A., Auger, C., Caldarelli, S. & Emsley, L. (1997) Determination of through-bond carbon− carbon connectivities in solid-state NMR using the INADEQUATE experiment. *Journal of the American Chemical Society*, **119**, 7867–7868.

Lesage, A., Charmont, P., Steuernagel, S. & Emsley, L. (2000) Complete resonance assignment of a natural abundance solid peptide by through-bond heteronuclear correlation solid-state NMR. *Journal of the American Chemical Society*, **122**, 9739–9744.

Liang, Y., Eudes, A., Yogiswara, S., Jing, B., Benites, V.T., Yamanaka, R. *et al.* (2019) A screening method to identify efficient sgRNAs in Arabidopsis, used in conjunction with cell-specific lignin reduction. *Biotechnology for Biofuels*, **12**, 130.

Lin, D., Lopez-Sanchez, P. & Gidley, M.J. (2015) Binding of arabinan or galactan during cellulose synthesis is extensive and reversible. *Carbohydrate Polymers*, **126**, 108–121.

Liwanag, A.J.M., Ebert, B., Verhertbruggen, Y., Rennie, E.A., Rautengarten, C., Oikawa, A. *et al.* (2012) Pectin biosynthesis: GALS1 in *Arabidopsis thaliana* is a β-1,4-galactan β-1,4-galactosyltransferase. *Plant Cell*, **24**, 5024–5036.

Loqué, D., Scheller, H.V. & Pauly, M. (2015) Engineering of plant cell walls for enhanced biofuel production. *Current Opinion in Plant Biology*, **25**, 151–161.

Mahajan, J.S., O'Dea, R.M., Norris, J.B., Korley, L.T.J. & Epps, T.H. (2020) Aromatics from lignocellulosic biomass: a platform for high-performance thermosets. *ACS Sustainable Chemistry & Engineering*, **8**, 15072–15096.

Makshakova, O.N., Gorshkova, T.A., Mikshina, P.V., Zuev, Y.F. & Perez, S. (2017) Metrics of rhamnogalacturonan I with β-(1→4)-linked galactan side chains and structural basis for its self-aggregation. *Carbohydrate Polymers*, **158**, 93–101.

Marriott, P.E., Gómez, L.D. & McQueen-Mason, S.J. (2016) Unlocking the potential of lignocellulosic biomass through plant science. *The New Phytologist*, **209**, 1366–1381.

McCartney, L., Ormerod, A.P., Gidley, M.J. & Knox, J.P. (2000) Temporal and spatial regulation of pectic (1→4)-beta-D-galactan in cell walls of developing pea cotyledons: implications for mechanical properties. *The Plant Journal*, **22**, 105–113.

Metz, G., Wu, X.L. & Smith, S.O. (1994) Ramped-amplitude cross polarization in magic-angle-spinning NMR. *Journal of Magnetic Resonance, Series A*, **110**, 219–227.

Mikshina, P.V., Gurjanov, O.P., Mukhitova, F.K., Petrova, A.A., Shashkov, A.S. & Gorshkova, T.A. (2012) Structural details of pectic galactan from the secondary cell walls of flax (*Linum usitatissimum* L.) phloem fibres. *Carbohydrate Polymers*, **87**, 853–861.

Moneo-Sánchez, M., Alonso-Chico, A., Knox, J.P., Dopico, B., Labrador, E. & Martín, I. (2019) β-(1,4)-galactan remodelling in Arabidopsis cell walls affects the xyloglucan structure during elongation. *Planta*, **249**, 351–362.

Moneo-Sánchez, M., Vaquero-Rodríguez, A., Hernández-Nistal, J., Albornos, L., Knox, P., Dopico, B. *et al.* (2020) Pectic galactan affects cell wall architecture during secondary cell wall deposition. *Planta*, **251**, 100.

Pattathil, S., Avci, U., Baldwin, D., Swennes, A.G., McGill, J.A., Popper, Z. *et al.* (2010) A comprehensive toolkit of plant cell wall glycan-directed monoclonal antibodies. *Plant Physiology*, **153**, 514–525.

Phyo, P., Wang, T., Xiao, C., Anderson, C.T. & Hong, M. (2017) Effects of pectin molecular weight changes on the structure, dynamics, and polysaccharide interactions of primary cell walls of *Arabidopsis thaliana*: insights from solid-state NMR. *Biomacromolecules*, **18**, 2937–2950.

Rennie, E.A. & Scheller, H.V. (2014) Xylan biosynthesis. *Current Opinion in Biotechnology*, **26**, 100–107.

Roach, M.J., Mokshina, N.Y., Badhan, A., Snegireva, A.V., Hobson, N., Deyholos, M.K. *et al.* (2011) Development of cellulosic secondary walls in flax fibers requires beta-galactosidase. *Plant Physiology*, **156**, 1351–1363.

Sandquist, D., Filonova, L., von Schantz, L., Ohlin, M. & Daniel, G. (2010) Microdistribution of xyloglucan in differentiating poplar cells. *BioResources*, **5**, 796–807.

Sawada, D., Kalluri, U.C., O'Neill, H., Urban, V., Langan, P., Davison, B. *et al.* (2018) Tension wood structure and morphology conducive for better enzymatic digestion. *Biotechnology for Biofuels*, **11**, 44.

Scheller, H.V., Jensen, J.K., Sørensen, S.O., Harholt, J. & Geshi, N. (2006) Biosynthesis of pectin. *Physiologia Plantarum*, **129**, 283–295.

Scheller, H.V. & **Ulvskov, P.** (2010) Hemicelluloses. *Annual Review of Plant Biology*, **61**, 263–289.

Simmons, T.J., **Mortimer, J.C.**, **Bernardinelli, O.D.**, **Pöppler, A.-C.**, **Brown, S.P.**, **de Azevedo, E.R.** ***et al.*** (2016) Folding of xylan onto cellulose fibrils in plant cell walls revealed by solid-state NMR. *Nature Communications*, **7**, 13902.

Sluiter, A., **Hames, B.**, **Ruiz, R.**, **Scarlata, C.**, **Sluiter, J.**, **Templeton, D.** ***et al.*** (2008) Determination of structural carbohydrates and lignin in biomass. Laboratory analytical procedure, Vol. **1617**, pp. 1–16. NREL, Denver, CO, USA. Technical Report NREL/TP-510-42618.

Smith, P.J., **Wang, H.-T.**, **York, W.S.**, **Peña, M.J.** & **Urbanowicz, B.R.** (2017) Designer biomass for next-generation biorefineries: leveraging recent insights into xylan structure and biosynthesis. *Biotechnology for Biofuels*, **10**, 286.

Sorek, N., **Yeats, T.H.**, **Szemenyei, H.**, **Youngs, H.** & **Somerville, C.R.** (2014) The implications of lignocellulosic biomass chemical composition for the production of advanced biofuels. *Bioscience*, **64**, 192–201.

Takegoshi, K., **Nakamura, S.** & **Terao, T.** (2001) ^{13}C–1H dipolar-assisted rotational resonance in magic-angle spinning NMR. *Chemical Physics Letters*, **344**, 631–637.

Tenhaken, R. & **Thulke, O.** (1996) Cloning of an enzyme that synthesizes a key nucleotide-sugar precursor of hemicellulose biosynthesis from soybean: UDP-glucose dehydrogenase. *Plant Physiology*, **112**, 1127–1134.

Terrett, O.M., **Lyczakowski, J.J.**, **Yu, L.**, **Iuga, D.**, **Franks, W.T.**, **Brown, S.P.** ***et al.*** (2019) Molecular architecture of softwood revealed by solid-state NMR. *Nature Communications*, **10**, 4978.

Wang, T. & **Hong, M.** (2016) Solid-state NMR investigations of cellulose structure and interactions with matrix polysaccharides in plant primary cell walls. *Journal of Experimental Botany*, **67**, 503–514.

Wang, T. & **Hong, M.** (2017) Structure and dynamics of polysaccharides in plant cell walls from solid-state NMR. In: Kato K, Peters T, eds. *NMR in glycoscience and glycotechnology*, London, UK: Royal Society of Chemistry, pp. 290–304.

Wang, T., **Park, Y.B.**, **Cosgrove, D.J.** & **Hong, M.** (2015) Cellulose-pectin spatial contacts are inherent to never-dried Arabidopsis primary cell walls: evidence from solid-state nuclear magnetic resonance. *Plant Physiology*, **168**, 871–884.

Wang, T., **Salazar, A.**, **Zabotina, O.A.** & **Hong, M.** (2014) Structure and dynamics of *Brachypodium* primary cell wall polysaccharides from two-dimensional (13)C solid-state nuclear magnetic resonance spectroscopy. *Biochemistry*, **53**, 2840–2854.

Wang, T., **Williams, J.K.**, **Schmidt-Rohr, K.** & **Hong, M.** (2015) Relaxation-compensated difference spin diffusion NMR for detecting ^{13}C-^{13}C long-range correlations in proteins and polysaccharides. *Journal of Biomolecular NMR*, **61**, 97–107.

Wang, T., **Yang, H.**, **Kubicki, J.D.** & **Hong, M.** (2016) Cellulose structural polymorphism in plant primary cell walls investigated by high-field 2D solid-state NMR spectroscopy and density functional theory calculations. *Biomacromolecules*, **17**, 2210–2222.

Wang, T., **Zabotina, O.** & **Hong, M.** (2012) Pectin-cellulose interactions in the Arabidopsis primary cell wall from two-dimensional magic-angle-spinning solid-state nuclear magnetic resonance. *Biochemistry*, **51**, 9846–9856.

Willats, W.G., **McCartney, L.**, **Mackie, W.** & **Knox, J.P.** (2001) Pectin: cell biology and prospects for functional analysis. *Plant Molecular Biology*, **47**, 9–27.

Wilson, S.M. & **Bacic, A.** (2012) Preparation of plant cells for transmission electron microscopy to optimize immunogold labeling of carbohydrate and protein epitopes. *Nature Protocols*, **7**, 1716–1727.

Xiao, C. & **Anderson, C.T.** (2013) Roles of pectin in biomass yield and processing for biofuels. *Frontiers in Plant Science*, **4**, 67.

Yan, J., **Aznar, A.**, **Chalvin, C.**, **Birdseye, D.S.**, **Baidoo, E.E.K.**, **Eudes, A.** ***et al.*** (2018) Increased drought tolerance in plants engineered for low lignin and low xylan content. *Biotechnology for Biofuels*, **11**, 195.

Yang, H., **Benatti, M.R.**, **Karve, R.A.**, **Fox, A.**, **Meilan, R.**, **Carpita, N.C.** ***et al.*** (2020) Rhamnogalacturonan-I is a determinant of cell–cell adhesion in poplar wood. *Plant Biotechnology Journal*, **8**, 1027–1040.

Zhu, P., **Abdelaziz, O.Y.**, **Hulteberg, C.P.** & **Riisager, A.** (2020) New synthetic approaches to biofuels from lignocellulosic biomass. *Current Opinion in Green and Sustainable Chemistry*, **21**, 16–21.

Zykwinska, A., **Rondeau-Mouro, C.**, **Garnier, C.**, **Thibault, J.-F.** & **Ralet, M.-C.** (2006) Alkaline extractability of pectic arabinan and galactan and their mobility in sugar beet and potato cell walls. *Carbohydrate Polymers*, **65**, 510–520.

Zykwinska, A., **Thibault, J.-F.** & **Ralet, M.-C.** (2007) Organization of pectic arabinan and galactan side chains in association with cellulose microfibrils in primary cell walls and related models envisaged. *Journal of Experimental Botany*, **58**, 1795–1802.

Zykwinska, A., **Thibault, J.-F.** & **Ralet, M.-C.** (2008) Competitive binding of pectin and xyloglucan with primary cell wall cellulose. *Carbohydrate Polymers*, **74**, 957–961.

Zykwinska, A.W., **Ralet, M.-C.J.**, **Garnier, C.D.** & **Thibault, J.-F.J.** (2005) Evidence for in vitro binding of pectin side chains to cellulose. *Plant Physiology*, **139**, 397–407.